

Article

# Air Mass Trajectories to Estimate the “Most Likely” Areas to Be Affected by the Release of Hazardous Materials in the Atmosphere—Feasibility Study

Miguel Ángel Hernández-Ceballos \*  and Luca De Felice 

European Commission, Joint Research Centre, 21027 Ispra, Italy; Luca.DE-FELICE@ec.europa.eu

\* Correspondence: miguelhceballos@gmail.com; Tel.: +39-033-278-3721

Received: 25 April 2019; Accepted: 7 May 2019; Published: 8 May 2019



**Abstract:** Countries continuously review and improve their Emergency Preparedness and Response (EP&R) arrangements and capabilities to take agile and rapid actions with the intent of minimizing health, environmental and economic impacts of potential harmful releases into the atmosphere. One of the specific topics within the EP&R field is the estimation of the areas that might be affected. A proposal is presented to estimate the spatial distribution of the released material. The methodology combines the computation of air mass trajectories and the elaboration of density maps from the corresponding end-point positions. To this purpose, density maps are created in a three-way procedure; first, forward trajectories are calculated from a certain location and for a long period of time, e.g., a decade; second, the selected end-point positions are aggregated in a density field by applying the kernel density estimation method, and then the density field is visualized. The final product reports the areas with the longest residence time of air masses, and hence, the areas “most likely” to be affected and where the deposit may be substantial. The usefulness of this method is evaluated taking as reference a ten-year period (2007–2016) and against two different radioactive release scenarios, such as the Chernobyl accident and the Algeciras release. While far from being fully comprehensive, as only meteorological data are used, the performance of this method is reasonably efficient, and hence, it is a desirable alternative to estimating those areas potentially affected by a substantial deposit following the releases of a harmful material in the atmosphere.

**Keywords:** Nuclear Emergency Preparedness and Response; air mass trajectory; density maps

## 1. Introduction

In the context of the effective management of crises and disasters, which is a global challenge, the risk of an accident releasing airborne harmful material to the atmosphere, like radioactive, chemical or bacteriological active substances, cannot be ruled out. To face these kinds of events, it is well recognized that good preparedness substantially improves the emergency response. In this line, efforts to promote and enhance global safety, and to limit and mitigate any consequences associated with these kinds of releases are continuously triggered at national and international levels [1].

The early phase of a harmful release to the atmosphere is a period usually characterized by large uncertainty in the source term release characteristics and the lack of field measurements. Within this period, to have available a prior estimation of the possible atmospheric transport and dispersion of the released material, and hence, the likely areas to be affected by the plume, is of importance to decision makers and emergency managers in an attempt at minimizing its health and environmental impacts.

Meteorological conditions determine the dispersion and transport of substances in the atmosphere. Rainfall, wind speed, wind direction and temperature are relevant parameters in establishing their temporal and spatial variability. Once in the atmosphere, the primary process favoring the transport

and dispersion of substances is wind regimes, which is characterized by wind direction and wind speed, e.g., the greater the wind velocity is, then the greater the dispersion of the contaminants, and the lower their concentration is [2]. Many studies [3,4] have outlined the need of characterizing wind regimes to understand air pollution scenarios. This direct link makes the knowledge and characterization of wind regimes at a site become key information in estimating the atmospheric transport and dispersion of harmful substances and, therefore, in forecasting the likely areas affected by the plume passage.

Air trajectory analysis is a central scientific tool to characterize synoptic and regional wind regimes [5]. The basic methodological approach in this kind of analysis is to generate massive amounts of air mass trajectories with the purpose of considering a large number of transport and dispersion scenarios so that the statistical analysis leads to the extraction of representative information about flow patterns (e.g., residence time, range, distance, speed, etc.). When compiled and studied over multiple years [6,7], the outcome of this trajectory analysis is used to generate an estimation of future wind scenarios.

With this in mind, the aim of this paper is to describe and to evaluate a method to estimate the likely areas to be affected by a hypothetical release to the atmosphere. The present methodology, which is based on the influence that lower atmosphere meteorology has on the dispersion and transport of substances in the atmosphere, is based on the calculation of density maps from air mass trajectories by applying the kernel density estimation (KDE) method [8]. KDE's strength is its ability to provide an estimate of density at any location in the spatial frame. In this present framework, these density maps report the areas with the longest residence time of air masses, and hence, the areas where the deposit may be substantial. Residence time analysis [9] identifies the likelihood that an air mass will traverse a given region in its movement to or from the site of interest over a given time period [7,10]. The longer the residence time over certain areas is, the more favorable the situation for significant surface dry deposition from contaminant plumes is.

Considering that the calculation of air mass trajectories is purely based on meteorological fields, i.e., we are not considering any release to the atmosphere (source term) in the calculation, we can only address a qualitative comparison to evaluate the outcomes of this method, e.g., between areas of high residence time and high deposit. To estimate the bias of this meteorological approach, we have evaluated it against the period 2006–2017 and two radioactive dispersion events, such as Chernobyl accident and Algeciras release. The corresponding density maps for each case study, which identify those areas with the longest residence time of air masses, are then qualitatively compared with those areas affected by high deposits in each release scenario. Reasonable estimation of the areas affected by both releases would prove the usefulness of this method and the number of years selected in the estimation of likely areas to be affected by a hypothetical release.

While far from being fully comprehensive of the complexity behind the simulation and prediction of atmospheric dispersion, as only meteorological data are used, this method would provide useful guidance in estimating the transport and dispersion that might result if harmful material reaches the atmosphere, and hence, in increasing knowledge of crisis and disaster management for improving responsiveness. Being only based on the analysis of the wind field, this method can be used, for instance, for any kind of airborne material.

The article is structured as followed. In Section 2, we describe the methodology applied to obtain density maps from air mass end-point positions, while Section 3 is dedicated to showing and discussing the results obtained in the two study cases taken as reference. To finalize, the conclusions obtained from this work are shown in Section 4.

## 2. Materials and Methods

### 2.1. Trajectory Modelling

Air mass trajectory shows the pathway of an infinitesimal air parcel through a centerline of an advected air mass having vertical and horizontal dispersion [11]. Forward trajectory estimates the pathway to be followed by an air parcel downwind from the selected coordinates in due course of time.

The National Oceanic and Atmospheric Administration (NOAA) Air Resources Laboratory's (ARL) Hybrid Single-Particle Lagrangian Integrated Trajectory model (HYSPLIT 4.9) [12] is used to calculate forward kinematic three-dimensional trajectories. The computation of three-dimensional trajectories is based on the use of the vertical velocity field included in publicly available meteorological datafiles, such as the 3-hourly meteorological archive data from NCEP's GDAS (National Weather Service's National Centers for Environmental Prediction-Global Data Assimilation System) [13]. The GDAS covers from 2004 to the present, which is a big advantage in favor of using them in research studies, as they span 10 years or more. The GDAS is run 4 times a day, i.e., at 0000, 0600, 1200, and 1800 UTC. These data are archived and made available by the NOAA's ARL as a global and 1-degree latitude–longitude dataset on pressure surface.

Our method uses forward trajectories with duration of 120 hours (length of the trajectory). A complete description of all the equations and HYSPLIT calculation methods for trajectories can be seen in [14]. HYSPLIT provides the coordinates (longitude and latitude) and height (in meters above ground level, a.g.l) of every trajectory calculated at 1-h intervals. Therefore, each trajectory of 120 h is composed of 120 end-point positions. In our study, we work these 120 end-point positions, which are the position of the lagrangian particles, at a certain hour within the duration of 120 h.

## 2.2. Kernel Density Estimation

Kernel density estimation (KDE) [8] is an important method in visualizing and analyzing spatial data, with application in many fields (ecology, public health, etc.), with the objective of understanding and potentially predicting event patterns [15–17]. KDE is a non-parametric approach to the estimation of probability density functions using a finite number of cases [18]. This method compensates for in distance the influence of a case in its vicinity. To this purpose, it incorporates a decay function that assigns smaller values to locations which are still in the neighborhood, but further way from a case [15]. To achieve this, KDE fits a curved surface over each case such that the surface is highest above the center and zero at a specified distance from the case (the bandwidth, i.e., the distance around a case at which its influence is felt). The influence of a number of cases at a certain location, over a two-dimensional space, can be represented as the following definition [8,19]:

$$f(x, y) = \frac{1}{nh^2} \sum_{i=1}^n K\left(\frac{d_i}{h}\right), \quad (1)$$

where  $f(x, y)$  is the density value at location  $(x, y)$ ,  $n$  is the total number of cases under concern,  $h$  is the bandwidth,  $d_i$  is the geographical distance between case  $i$  and the location and  $K$  is a density function (generally a radially symmetric unimodal probability density function) which integrates to one. Different density functions ( $K$ ) can be used, e.g., Cauchy [20], Epanechnikov [21], Gaussian [22]. More information about different kernel-smoothing algorithms can be found in [23].

The KDE refers to high or low density of points, i.e., cases per unit area. Therefore, KDE method detects the highs and lows of cases densities of the pattern, and is useful for detecting hot spots. Figure 1 graphically shows an example of the procedure use in our method to determine the density value  $f(x, y)$  (grey squared) over the raster data by considering two cases (red circles).

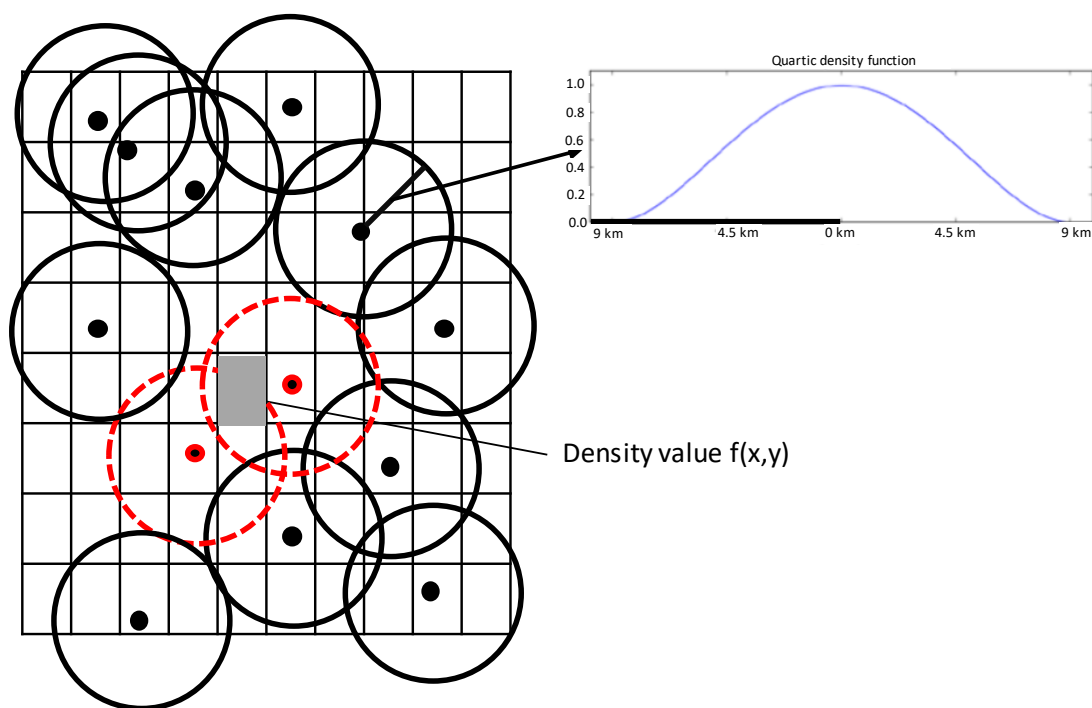


**Figure 1.** An illustration of the density value  $f(x,y)$  calculations over raster data and the quartic kernel function used ( $K$ ), with a bandwidth of 9 km.

### 2.3. Method

Figure 2 shows the procedure applied in our method to determine the corresponding density maps. Once calculated, the trajectories for the period 2007–2016 (Figure 2a), and the corresponding end-point positions (i.e., cases in Section 2.2), the subset of end-point positions within the analyzed period (hereafter, time window), are extracted (Figure 2b). We define the “time window” as the reference period for which end-point positions are collected and to which, as a result, the density map refers. This time window refers to one reference time (e.g., a specific day, such as the release date or the maximum concentration date). The definition of the time window is based on the fact of having evidences that cyclicity plays a significant role in the weather we experience, i.e., weather appears to be a regularly cycling pattern over short and long-range time. In the present method, we consider three different temporal cycling patterns of weather, e.g., two weeks, one month and two months. As an example, if the event date is 7 May, we work with all end-point positions within the period 2007–2016 from 1 May to 14 May (one week before and after the release date), from 24 April to 21 May (two weeks before and after), and from 7 April to 7 June (one month before and after).

Based on the end-point positions extracted, we provide a comprehensive analysis of the residence time of air masses. In order to accommodate as much as possible the residence time with hypothetical deposits from the plume, the present analysis is carried out by selecting the number of end-point positions below a vertical level, which is set to 100 m a.g.l., within the selected time window

Once the subset of end-point positions within the time window and with a height less than 100 m a.g.l are selected, these are then displayed as a density map using the KDE method indicated in Section 2.2 (Figure 2c,d). To make a KDE, the challenge is to select the kernel function, the bandwidth and the cell size. However, there are no rules and standards concerning this selection, and they are predominantly taken as the results of experimental studies [24]. After several analyses, in the present work, end-point positions are displayed on a map with a fixed grid cell size of  $3 \times 3$  km and we have defined a bandwidth of 9 km, while the kernel function is based on the quartic kernel function described in [8], i.e., an inverse distance weighting (Figure 1). We have used the free and open source QGIS geographic information system [25].

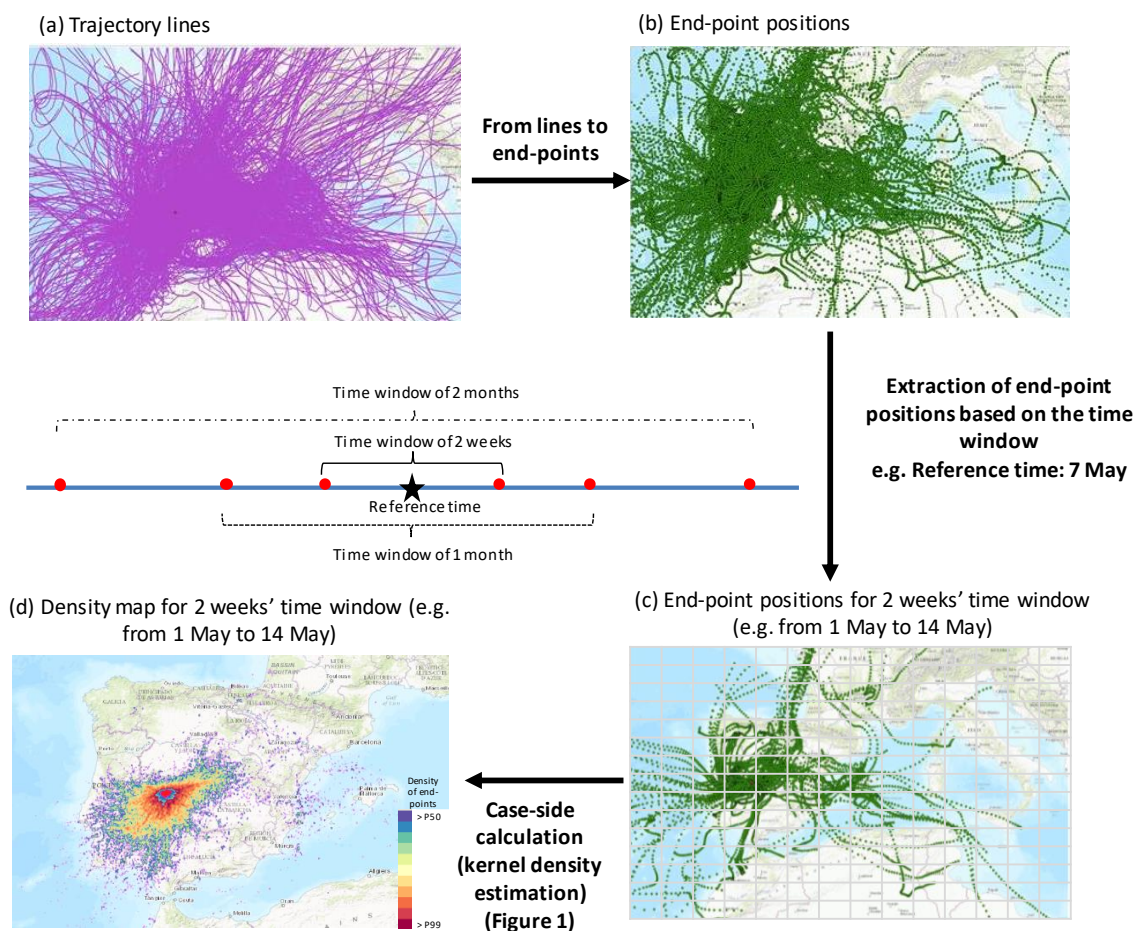


**Figure 2.** Steps and information used to produce the density maps: (a) Set of trajectory lines, (b) end-point positions for the 2007–2016 period, (c) definition of time windows and extraction of end-point positions for the defined time window (2 weeks) and (d) example of density map, which expresses the density of end-point positions estimated above 50%.

### 3. Case Studies

Two case studies, the Chernobyl accident (25–26 April 1986) and the Algeciras release (30 May 1998), have been taken as reference in order to evaluate the use of trajectories and density maps as valuable information in the preparedness phase of an atmospheric event release.

An explosive accident took place at the Chernobyl nuclear power plant unit IV in Ukraine on 25 April 1986 at 2123 UTC. This accident led to a widespread dispersion of radioactive materials released at different times in the atmosphere at a continental scale. The meteorological conditions caused the various plumes to take different directions according to the release date [26], and therefore, contaminated clouds flew all around the world.

On 30 May, 1998, a  $^{137}\text{Cs}$  medical source was accidentally melted in one of the furnaces at the Acerinox stainless steel production plant near Algeciras, southern Spain. An unknown amount of contaminated air was dispersed over the western coast of Spain and travelled all the way north, reaching the southern coast of France and northern Italy two to three days after the release. The International Atomic Energy Agency (IAEA) Emergency Response Centre reported the occurrence of a radiological accident on June 12.

Following the methodology explained in Section 2.3, we have calculated the forward trajectories and the corresponding end-point positions for the 10-year period (2007–2016) at Chernobyl ( $51^{\circ}23'23.47''$  N,  $30^{\circ}5'38.57''$  E) and Algeciras ( $6^{\circ}7'39''$  N,  $5^{\circ}27'14''$  W).

In accordance with the release characteristic of each release scenario [27,28], the initial height applied in the calculation of trajectories differs: Chernobyl at 1000 m a.g.l and Algeciras release at 100 m a.g.l. For each scenario, over 97% of 1-h trajectories in the period 2007–2016 are completed for all 120 h (an incomplete trajectory is due to missing data in the initialization fields).

Table 1 shows the three time windows defined for each case study, taking as reference the corresponding release date to calculate the associated density map.

**Table 1.** Time windows defined for Chernobyl and Algeciras case studies to extract the end-point positions in the period 2007–2016.

	Time Window of Two Weeks	Time Window of One Month	Time Window of Two Months
Chernobyl (reference date: 25 April)	From 18 April to 3 May	From 11 April to 9 May	From 25 March to 25 May
Algeciras (reference date: 30 May)	From 23 May to 6 June	From 16 May to 13 June	From 30 April to 30 June

#### 4. Results and Discussion

This section presents the set of density maps calculated for each case study. To evaluate the bias of our meteorological approach, the results obtained in the density maps are qualitatively compared with bibliography regarding the depositional analysis of each case study. We need to point out that our method does not aim to estimate the deposit, but the areas affected.

##### 4.1. Chernobyl Accident

Figure 3 shows the density maps produced applying each one of the three time windows (Table 1) for the period 2007–2016 from the Chernobyl site. The three maps display a large spatial dispersion from the release point. Our analysis finds high-density values (above the 90th percentile, P90) in central Europe and Scandinavia. This large dispersion provides an example of the differences in flow regimes, with areas being affected to the south (from southwest to southeast) and to the north of the release point. This spatial spread is in agreement with the variation in the meteorological conditions according to the release date. The emissions on 26 April were transported in the western and northern directions [29], while the plume released in the following days started to move in a south-westerly direction, towards central Europe [30], as well as towards Asia [31].

The highest density values (above the 99th Percentile (P99); the blue circles in Figure 3) in the three density maps are located to the southwest of the source region. This region covers areas of Romania and Bulgaria, such as the Western Romanian Carpathians, as well as the landmass formed inside the mountain circle, the Transylvanian Plateau and the Western Plain and Hills. The geographical distribution of elevated residence times in Figure 3 is in agreement with most of the areas identified in the “Atlas of cesium deposition on Europe after the Chernobyl accident” [32]. Figure 4 shows the high-resolution map of the total cumulative deposition of  $^{137}\text{Cs}$  throughout Europe as a result of the Chernobyl accident, which is used in this paper to validate the areas identified in Figure 3. Figure 4 shows that high deposits occurred in Eastern Europe and the Balkan countries, following the dominant precipitation. These areas are well identified in our density maps, which report the highest residence time values on the northern and southern borders of Romania.

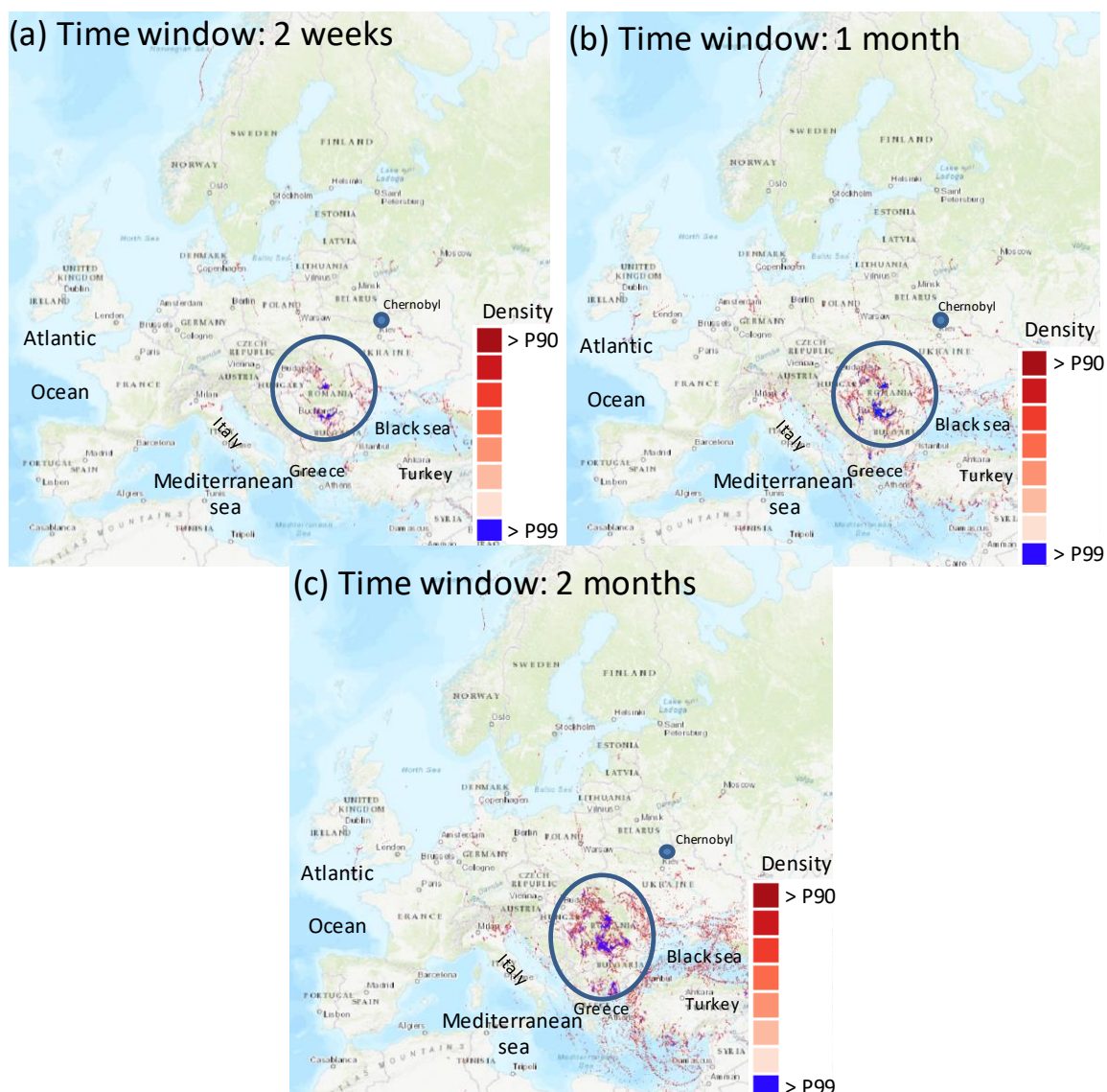


**Figure 3.** Density plots for 120-h trajectories starting at Chernobyl (blue point) and with a height below 100 m above ground level for (a) 2 weeks, (b) 1 month and (c) 2 months' time window (reference date of April 25) for the period 2007–2016 (Table 1). The density maps express the density of end-point positions estimated above 90%; quartic kernel function bandwidth 9 km. Blue circles express those areas with a density value above the 99th percentile.

Comparing the three maps (Figure 3), the area with the highest density values is better identified on increasing the time window from two weeks to two months, i.e., the number of end-point positions, and hence, the meteorological scenarios. The impact of the time window on results is well observed by comparing the greater spread of spots with values above P90 between Figure 3a (time window of two weeks) and Figure 3c (time window of two months). This impact is especially seen to the south of the release site, as high-density values show up in the Black and Aegean seas, and northern Italy–southern Austria. In addition, zones in northern Germany and in the United Kingdom are identified by using a longer time window. In contrast, the set of areas identified in northern countries does not vary with the time window. In this region, few spots can be identified over continental areas, such as southern and eastern coastal areas of Sweden. In contrast, Figure 4 displays a large spread of high  $^{137}\text{Cs}$  in specific areas of Sweden and Finland. One of the reasons of this difference can be associated with the selection of density values up to P90.

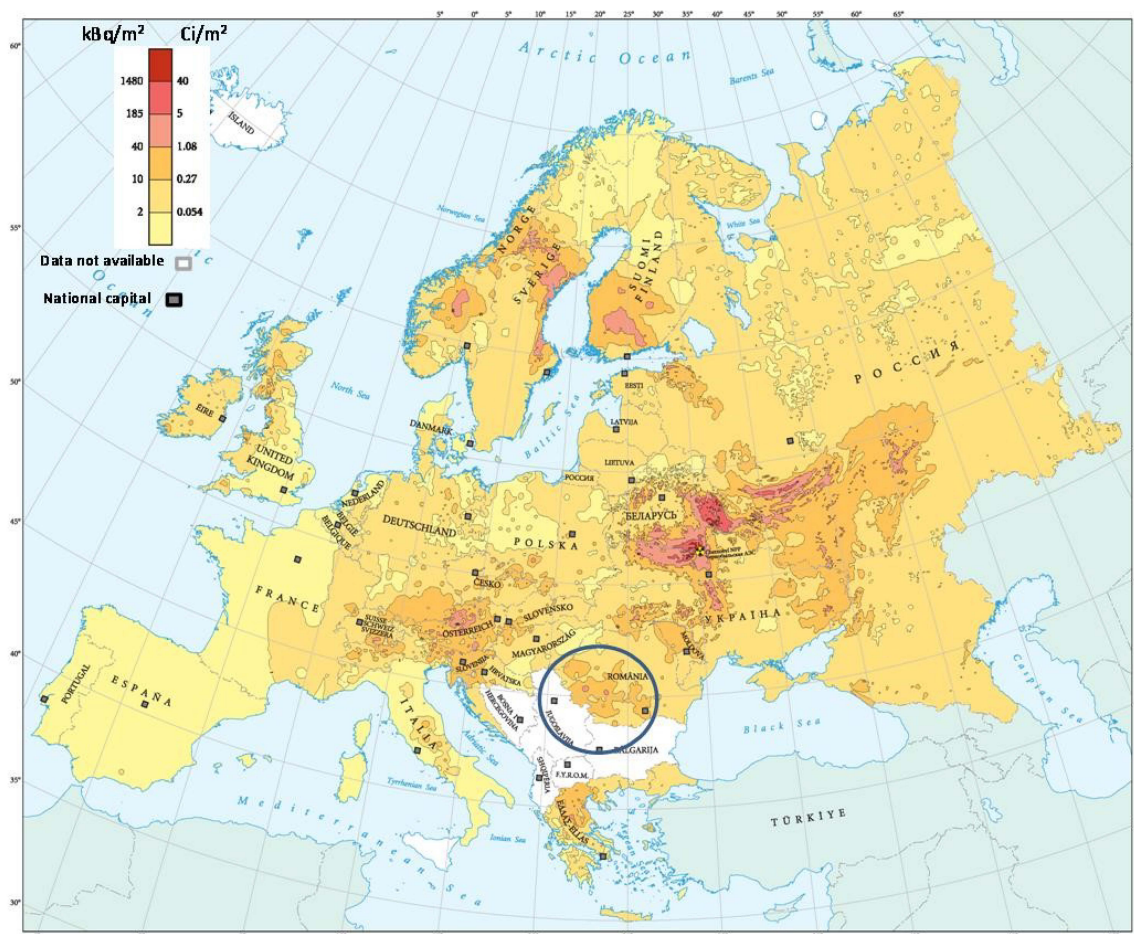


**Figure 4.** The Atlas map (using the Lambert azimuthal projection) depicting the total cumulative deposition of <sup>137</sup>Cs throughout Europe as a result of the Chernobyl accident from all available data of the REM database corrected for radioactive decay to 10 May 1986 [31]. Blue circle expresses the areas with a density value above the 99th Percentile obtained in Figure 3.

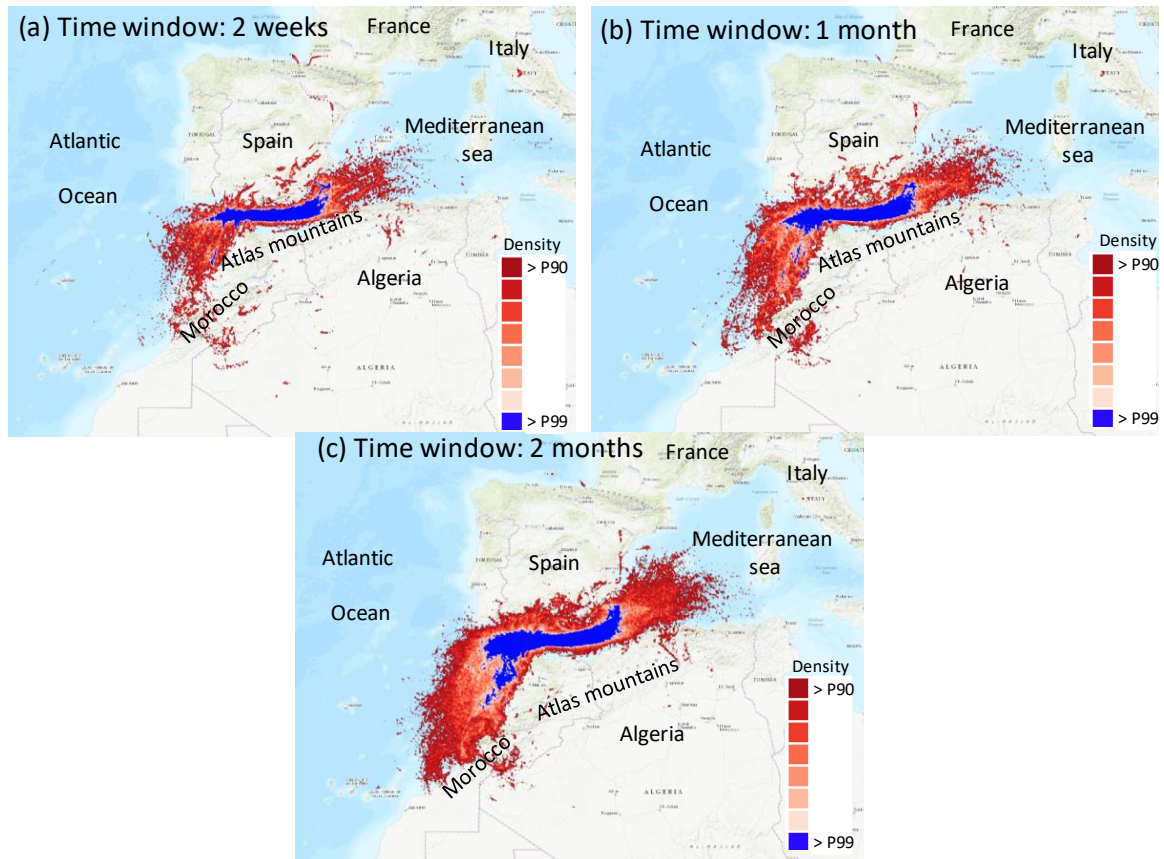
#### 4.2. Algeciras Release

Figure 5 shows the corresponding density maps for the three time windows defined for the Algeciras case study. Density maps look similar for the three “time windows”, with the increase in the most affected area (>P90) easily seen by increasing the time window considered. The trajectories have either an eastern or southwestern component, displaying two main branches of the possible dispersion of the plume released at Algeciras. While the branch to the east, over the Alboran Sea, turns to the northeast following the Spanish coastline, the one to the west veers to the southwest following the northwestern coast of Africa. In both cases, after the channeling effect created by the southern Iberian Peninsula and northern African mountain chains, there is a wide area over the Atlantic and Mediterranean covered by high-density values.

The three maps display a wider area corresponding to the highest density values (above P99) to the east of the release site, along the southern Mediterranean coast of the Iberian Peninsula. It is interesting to highlight how this Mediterranean branch also presents areas over central Italy and northern Africa with high-density values.

This distribution is completely in agreement with the wind dynamics in this area, which is clearly conditioned by the channeling effect of the strait of Gibraltar [33]. The highest density values are obtained to the east of the release site, over the Mediterranean Sea, being consistent with previous studies dealing with this event [34], which reported an easterly movement of the plume. According to the measurements of <sup>137</sup>Cs registered in southern France and northern Italy at the beginning of June,

the radioactive plume continued its movement to the north-west over the Mediterranean Sea the following days. The density maps suggest this displacement, although the consideration of trajectories with a duration of 120 h limits the possible identification of continental areas affected.



**Figure 5.** Density plots for 120-h trajectories starting at Algeciras and with a height below 100 m above ground level for (a) 2 weeks, (b) 1 month and (c) 2 months' time window (reference date of 30 May) for the period 2007–2016 (Table 1). The density maps express the density of end-point positions estimated above 90%; quartic kernel function bandwidth 9 km.

## 5. Conclusions

This paper addresses the method developed to estimate the areas that could be most affected by harmful airborne releases to the atmosphere. To the author's knowledge, this is the first study in which a long-term set of trajectories is used as part of an emergency preparedness infrastructure to early estimate areas likely to be affected by the release of harmful substances in the atmosphere. The bases for this approach are 5-days forward trajectories departing every 1 h at different heights above ground (in accordance with the study case) for the period 2007–2016.

We have qualitatively evaluated the method by comparing the results from density maps against the air concentration and deposition maps of  $^{137}\text{Cs}$  from the Chernobyl and Algeciras releases. The comparison reports a reasonable agreement in the identification of both the atmospheric dispersion patterns and the areas most affected by  $^{137}\text{Cs}$  activity concentrations.

Differences in the spatial coverage of the potential affected areas between these two events highlight the influence of the orography and of the release height in the transport and dispersion of substances in the atmosphere. While in Chernobyl (initial height of 1000 m a.g.l.), the transport occurs mainly above the boundary layer (1–2 km above surface) and hence, surface features affect the wind less (e.g., frictional drag); in Algeciras the wind is forced to move in a certain direction by the presence of mountains. In this sense, the Chernobyl map is a good example of the orographic blocking caused

by the mountains, forcing the winds to slow down and/or change direction much more. The highest density values for the Chernobyl case study are found within the arc of the Carpathians and in the southern part of the country, in the Danube Plain, between the sub-Carpathians and Balkans. The main transport direction in the Algeciras case study is to the east, in agreement with previous studies.

The comparisons of density maps produced by different time windows (from weeks to months) have shown similarities in the identification of areas highly affected (>P99) by the air mass passage. The use of long time windows has produced the increase of the spatial coverage of these areas, but not the clear identification of new ones. The use of long time windows (more than one week before and after the release date), therefore, could not be necessary, as it could include the consideration of inhomogeneous and noisy trajectory endpoints.

While this method is far from being fully comprehensive, as only meteorological data are used, by building on the current results, future work with the purpose of including more years and measured concentrations into the analysis will help to further improve the present method, and to perform a quantitative evaluation.

**Author Contributions:** Conceptualization, M.Á.H.-C.; methodology, M.Á.H.-C. and L.D.F; formal analysis, M.Á.H.-C. and L.D.F; investigation, M.Á.H.-C. and L.D.F; resources, M.Á.H.-C. and L.D.F; visualization, L.D.F; data curation, L.D.F; writing—original draft preparation, M.Á.H.-C.; writing—review and editing, M.Á.H.-C. and L.D.F; supervision, M.Á.H.-C.

**Funding:** This research received no external funding.

**Acknowledgments:** The authors gratefully acknowledge the NOAA Air Resources Laboratory (ARL) for the provision of the HYSPLIT transport and dispersion model and/or READY website (<http://www.ready.noaa.gov>) used in this publication. The authors also acknowledge the Open Source Geospatial Foundation (OSGeo) for the provision of the QGIS project.

**Conflicts of Interest:** The authors declare no conflict of interest.

## References

1. International Atomic Energy Agency (IAEA). *Preparedness and Response for a Nuclear or Radiological Emergency*; IAEA Safety Standards Series No. GSR Part 7; IAEA: Vienna, Austria, 2015.
2. Cooper, J.R.; Randle, K.; Sokhi, R.S. *Radioactive Releases in the Environment: Impact and Assessment*; John Wiley & Sons: Hoboken, NJ, USA, 2003; ISBN 978-0-471-89924-2.
3. Yang, X.; Wang, T.; Xi, M.; Gao, X.; Li, Q.; Zhang, N.; Gao, Y.; Lee, S.; Wang, X.; Xye, L.; et al. Abundance and origin of fine particulate chloride in continental China. *Sci. Total. Environ.* **2018**, *624*, 1041–4051. [[CrossRef](#)]
4. Wang, W.; Yu, J.; Cui, Y.; He, J.; Xue, P.; Cao, W.; Ying, H.; Gao, W.; Yan, Y.; Hu, B.; et al. Characteristics of fine particulate matter and its sources in an industrialized coastal city, Ningbo, Yangtze River Delta, China. *Atmos. Res.* **2018**, *203*, 105–117. [[CrossRef](#)]
5. Pérez, I.A.; Artuso, F.; Mahmud, M.; Kulshrestha, U.; Sánchez, M.L.; García, M.A. Applications of Air Mass Trajectories. *Adv. Meteorol.* **2015**. [[CrossRef](#)]
6. Toledano, C.; Cachorro, V.E.; De Frutos, A.M.; Torres, B.; Berjón, A.; Sorribas, M.; Stone, R.S. Airmass classification and analysis of aerosol types at El Arenosillo (Spain). *J. Appl. Meteorol. Climatol.* **2009**, *48*, 962–981. [[CrossRef](#)]
7. Hondula, D.M.; Sitka, L.; Davis, R.E.; Knight, D.B.; Gawtry, S.D.; Deaton, M.L.; Lee, T.R.; Normile, C.P.; Stenger, P.J. A back-trajectory and air mass climatology for the Northern Shenandoah Valley, USA. *Int. J. Climatol.* **2010**, *30*, 569–581. [[CrossRef](#)]
8. Silverman, B.W. *Density Estimation for Statistics and Data Analysis*; Chapman and Hall: New York, NY, USA, 1986.
9. Ashbaugh, L.L. A statistical trajectory technique for determining air pollution source regions. *APCAJ* **1983**, *33*, 1096–1098. [[CrossRef](#)]
10. Fleming, Z.L.; Monks, P.S.; Manning, A.J. Review: Untangling the influence of air-mass history in interpreting observed atmospheric composition. *Atmos. Res.* **2012**, *104–105*, 1–39. [[CrossRef](#)]
11. Kulshrestha, U.; Kumar, B. Airmass Trajectories and Long Range Transport of Pollutants: Review of Wet Deposition Scenario in South Asia. *Adv. Meteorol.* **2014**. [[CrossRef](#)]

12. Stein, A.F.; Draxler, R.R.; Rolph, G.D.; Stunder, B.J.B.; Cohen, M.D.; Ngan, F. NOAA's HYSPLIT atmospheric transport and dispersion modeling system. *Bull. Amer. Meteor. Soc.* **2015**, *96*, 2059–2077. [[CrossRef](#)]
13. Meteorological Archive Data from NCEP's GDAS. Available online: <https://www.ready.noaa.gov/gdas1.php> (accessed on 20 January 2019).
14. Draxler, R.; Hess, G. *Description of the HYSPLIT\_4 Modeling System*; National Oceanic and Atmospheric Administration: Silver Spring, MD, USA, 1997.
15. Carlos, H.A.; Shi, X.; Sargent, J.; Tanski, S.; Berke, E.M. Density estimation and adaptive bandwidths: A primer for public health practitioners. *Int. J. Health Geogr.* **2010**, *9*, 39. [[CrossRef](#)]
16. Smith, M.-J.; Goodchild, M.-F.; Longley, P.-A. *Geospatial Analysis: A Comprehensive Guide to Principles; Techniques and Software Tools*; The Winchelsea Press: Winchelsea, UK, 2015.
17. Bartolini, S.; Cappello, A.; Marti, J.; Del Negro, C. QVAST: A new Quantum GIS plugin for estimating volcanic susceptibility. *Nat. Hazards Earth Syst. Sci.* **2013**, *13*, 3031–3042. [[CrossRef](#)]
18. Krisp, J.M.; Peters, S.; Murphy, C.E.; Fan, H. Visual Bandwidth Selection for Kernel Density Maps. *Photogramm. Fernerkund. Geoinf.* **2009**, *5*, 441–450. [[CrossRef](#)]
19. Shi, X. Selection of bandwidth type and adjustment side in kernel density estimation over inhomogeneous backgrounds. *J. Int. J. Geogr. Inf. Sci.* **2010**, *24*, 643–660. [[CrossRef](#)]
20. Martin, A.J.; Umeda, K.; Connor, C.B.; Weller, J.N.; Zhao, D.; Takahashi, M. Modeling long-term volcanic hazards through Bayesian inference: An example from the Tohoku volcanic arc Japan. *J. Geophys. Res.* **2004**, *109*. [[CrossRef](#)]
21. Lutz, T.M.; Gutmann, J.T. An improved method for determining and characterizing alignments of point-like features and its implications for the Pinacate volcanic field, Sonoran, Mexico. *J. Geophys. Res.* **1995**, *100*, 17659–17670. [[CrossRef](#)]
22. Connor, C.B.; Hill, B.E. Three nonhomogenous Poisson models for the probability of basaltic volcanism: Application to the Yucca Mountain region, Nevada. *J. Geophys. Res.* **1995**, *100*, 10107–10125. [[CrossRef](#)]
23. Wand, M.P.; Jones, M.C. *Kernel Smoothing Monographs on Statistics and Applied Probability*; Chapman & Hall/CRC: Taylor & Francis Group: Boca Raton, FL, USA, 1995.
24. Wolf, M.; Asche, H. Exploring Crime Hotspots: Geospatial Analysis and 3D Mapping. In Proceedings of the 14th International Conference on Urban Planning, Regional Development and Information Society, Schwechat, Austria, 22–25 April 2009.
25. QGIS Development Team. QGIS Geographic Information System. *Open Source Geospatial Foundation*. Available online: <http://qgis.org> (accessed on 20 September 2018).
26. Institute De Radioprotection et de Surete Nucleaire (ISRN), Chernobyl 25 years on. 2011. Available online: [https://www.irsn.fr/EN/publications/thematicsafety/chernobyl/Documents/irsn\\_booklet\\_chernobyl\\_2011.pdf](https://www.irsn.fr/EN/publications/thematicsafety/chernobyl/Documents/irsn_booklet_chernobyl_2011.pdf) (accessed on 10 January 2019).
27. Bartnicki, J.; Salbu, B.; Saltbones, J.; Foss, A.; Lind, O.L. *Gravitational Settling of Particles in Dispersion Model Simulations Using the Chernobyl Accident as a Test Case*; Research Report; Norwegian Meteorological Institute: Oslo, Norway, 2001; ISSN 0332-9879.
28. Kaviani, F.; Memarian, M.H.; Eslami-Kalantari, M. Simulation of atmospheric dispersion, transport and deposition of nuclear pollutants released from a hypothetical accident at Bushehr Power Plant. *J. Earth Space Phys.* **2017**, *43*, 635–650. [[CrossRef](#)]
29. Langner, J.; Robertson, L.; Persson, C.; Ullerstig, A. Validation of the operational emergency response model at the Swedish meteorological and hydrological institute using data from ETEX and the Chernobyl accident. *Atmos. Environ.* **1998**, *32*, 4325–4333. [[CrossRef](#)]
30. Talerko, N. Mesoscale modelling of radioactive contamination formation in the Ukraine caused by the Chernobyl accident. *J. Environ. Radioact.* **2005**, *78*, 311–329. [[CrossRef](#)] [[PubMed](#)]
31. Simsek, V.; Pozzoli, L.; Unal, A.; Kindap, T.; Karaca, M. Simulation of <sup>137</sup>Cs transport and deposition after Chernobyl Nuclear Power Plant accident and radiological doses over the Anatolian Peninsula. *Sci. Total Environ.* **2014**, *499*, 74–88. [[CrossRef](#)] [[PubMed](#)]
32. De Cort, M.; Dubois, G.; Fridman, S.D.; Germenchuk, M.G.; Izrael, Y.A.; Janssens, A.; Jones, A.R.; Kelly, G.N.; Kvasnikova, E.V.; Matveenko, I.I.; et al. *Atlas of Caesium Deposition on Europe after the Chernobyl Accident*; Office of the European Union: Luxembourg, 1998; p. 176.

33. Dorman, C.E.; Beardsley, R.C.; Limeburner, R. Winds in the strait of Gibraltar. *Quarterly J. R. Meteorol. Soc.* **1995**, *121*, 1093–1921. [[CrossRef](#)]
34. Vogt, P.J.; Pobanz, B.M.; Aluzzi, F.J.; Baskett, R.L.; Sullivan, T.J. ARAC Modeling of the Algeciras, Spain Steel Mill CS-137 Release. Available online: <https://www.osti.gov/servlets/purl/15013432> (accessed on 20 January 2019).



© 2019 by the authors. Licensee MDPI, Basel, Switzerland. This article is an open access article distributed under the terms and conditions of the Creative Commons Attribution (CC BY) license (<http://creativecommons.org/licenses/by/4.0/>).